Mars Initial Reference Ionosphere (MIRI) Model: Updates and Validations using MAVEN, MEX, and MRO Data Sets

Michael Mendillo[1], Clara Narvaez[1], Jeffrey Trovato[1], Paul Withers[1], Majd Mayyasi[1], David Morgan[2], Andrew Kopf[2], Donald Gurnett[2], Frantisek Němec[3] and Bruce Campbell[4]

[1]Center for Space Physics, Boston University, Boston, Massachusetts, USA.

[2]Department of Physics and Astronomy, The University of Iowa, Iowa City, Iowa, USA.

[3]Faculty of Mathematics and Physics, Charles University, Prague, Czech Republic.

[4]Center for Earth and Planetary Studies, Smithsonian Institution, MRC 315, PO Box 37012, Washington, DC, USA.

Corresponding author: Clara Narvaez (cnarvaez@bu.edu)

Key Points:

- Scientific understanding of complex ionospheric patterns and processes at Mars requires a baseline specification model
- New methods of daily predictions for maximum electron density and total electron content are derived and tested using new data sets
- Validation issues for mid-day conditions require more accurate theoretical calculations of X-ray produced secondary ionization rates

This article has been accepted for publication and undergone full peer review but has not been through the copyediting, typesetting, pagination and proofreading process which may lead to differences between this version and the Version of Record. Please cite this article as doi: 10.1029/2018JA025263

Abstract

The Mars Initial Reference Ionosphere (MIRI) Model is a semi-empirical formulation designed to provide climatological estimates of key parameters of the Martian ionosphere. For the new MIRI-2018 version, an expanded data base is used from the MEX/MARSIS/AIS instrument, consisting of 215,818 values of maximum electron density of the M2-layer (N_mM_2) from the years 2005-2015. These data are organized by photo-chemical-equilibrium equations to obtain a functional dependence of N_mM_2 upon solar drivers (flux and solar zenith angle). The resulting peak density is used to calibrate normalized electron density profiles [$N_e(h)$] derived from theory and an empirical model. The MIRI-2018 thus provides estimates of N_mM_2, $N_e(h)$ and total electron content (TEC) for any date past or future. Validation using MAVEN's new radio occultation science experiment (ROSE) was successful for N_mM_2 values, but MIRI was found to over-estimate TEC values. The validation failure for TEC was traced to over-estimates of plasma at low altitudes (M1-layer). A separate module for TEC was derived using 126,055 values from the MRO/SHARAD TEC data base from 2006-2014. Validation of this new TEC module with ROSE data was successful. Future improvements to MIRI-2018 require new ways to characterize the bottomside ionosphere's contribution to the TEC integral for midday (low solar zenith angle) conditions. This requires new simulation studies of secondary ionization rates by photo-electrons produced via the primary X-ray ionization process for the M1-layer.

1 Introduction

Models of a planet's ionosphere fall into three general categories: (a) First-principle theoretical models, (b) Empirical models, and (c) Semi-empirical models. The theoretical models can be 1-dimensional vertically, 2-dimensional (meridional) in height and latitude, and 3-dimensional using height, latitude and longitude—with all as a function of local time. The empirical models use mathematical fits to large data bases to characterize 1-, 2- and 3-D patterns in space and time, while the semi-empirical models organize data by equations from theory. For Mars, examples of (a) are global circulation models (Bougher et al., 2015; Chaufray et al., 2014) and MHD codes (Ma et al., 2004) for 3-D results and Matta et al. (2015) for a 2-D model. There are many examples for 1-D models (Martinis et al., 2003; Fox, 2004; Mayyasi & Mendillo, 2015, and references therein). For (b), data-driven 1-D models are typified by the approaches of Sanchez-Cano et al. (2015) and Němec et al. (2016). For (c), the MIRI approach to be described here uses photo-chemical-equilibrium (PCE) theory as the framework for transforming observations into predictive schemes (Mendillo et al., 2013). While theoretical models provide results ranging from general climatology to "tailored-runs" for case-studies of a specific day, the data-driven and semi-empirical MIRI models strive to offer quick-look "expectations" of the ionosphere at Mars for any day between 1 Jan, 1964 and 31 Dec, 2019 (using predicted solar fluxes).

2 Why a Reference Ionosphere Model?

The fundamental goal of an interactive model of the Martian ionosphere is to enable scientific studies of the processes that control the planet's cold plasma environment. The goal for MIRI is to provide a daily climatology of the electron density profile [$N_e(h)$] and its integral (total electron content, TEC). MIRI predictions provide a way to assess if new observations offer typical or unusual descriptions of the ionosphere. For example, do new data sets serve as validations of previous knowledge or do they reveal new ionospheric structures in need of follow-up studies? Conversely, new observations (or the synthesis of many previous data sets) may not agree with predictions from a reference ionosphere model due to shortfalls in the model. In such cases, additional studies are needed of the physical

processes included in MIRI that came from parameterizations of previously-published first-principle models. For example, one of the conclusions to be presented below is that the MIRI-2018 predictions of electron density in Mars' M1-layer contribute an unusually large portion of the total electron content (TEC) under mid-day conditions. This implies that new methods are needed in current theoretical models that attempt to characterize secondary ionization produced by photo-electrons as a multiplicative factor applied to primary ionization by soft X-rays under small solar zenith angle conditions.

A reference ionosphere model also has scientific uses beyond electron density and TEC investigations. MIRI can also be used to compute optical emissions from ion-electron recombination and/or plasma-neutral chemical reaction processes. Such calculations aid in the interpretation of optical aeronomy data sets (or planning for them). Electrical conductivities play a major role in simulations of electro-dynamical effects included in first-principle general circulation models and in MHD codes. MIRI's $N_e(h)$ profiles from 80-400 km offer a method to do so (with assumptions about ion compositions).

Separate from the few scientific examples given above, a reference ionosphere model also provides a source of information relevant to application needs. These include, for example, the background ionosphere needed to conduct ray-tracing for radiowaves linking satellite and surface transmitters/receivers that are part of global navigation and communication systems.

3 The MIRI Approach

The ionosphere at Mars is dominated by photo-chemical-equilibrium (PCE) processes from its lowest altitudes near 80 km to heights of ~170 - 200 km (Bauer, 1973). The maximum electron density occurs at heights ~130 km, and thus well within the PCE domain. For nomenclature, Bauer (1973) suggested that ionospheric layers should be defined by the portion of the solar irradiance (photon flux versus wavelength) that produced them. With Earth setting the precedent, soft X-rays create the low altitude E-layer and EUV the F1-layer above it. Inherent in this definition was the designation of maximum electron densities (NmE and NmF1) produced under conditions of photo-chemical-equilibrium (PCE)—chemistry without plasma dynamics. Thus, every planet in our solar system has an E-layer and and F1-layer.

The F1-layer produced at Mars conforms to PCE conditions at its height of maximum electron density (h_{max}). Non-PCE effects of plasma diffusion and electro-dynamical transport occur in the topside ionosphere from heights of ~170 km to its termination by the solar wind. Such "ionopause" heights can occur in the 250-400 km range (Vogt et al., 2015; Mendillo et al., 2015; Mendillo, Narvaez, Vogt, Mayyasi, Mahaffy, et al., 2017). This topside dynamical ionosphere at Mars is vastly different from the PCE-only topside F1-layer at Earth, and thus the use of terrestrial terminology defined by peak densities presents an inconsistency. MIRI deals with the full electron density profile and its integral (total electron content). The designation of the Martian ionosphere as the sum of terrestrial-type E+F1 layers does not capture the combined nature of PCE plus dynamics. We thus adopt for MIRI the more generic terms introduced by Rishbeth and Mendillo (2004) for the low-altitude layer (M1) and primary layer (M2) above it. The results to follow do not depend on this choice of terminology.

Within the photo-chemical domain, electron densities result from the balance of plasma production and loss. The ion-electron recombination chemistry that defines loss depends weakly on the value of electron temperature (T_e), and thus day-to-day changes in the maximum electron density of the M2-layer (N_mM_2) due to electron temperature variability are small (Mendillo, Narvaez, Vogt, Mayyasi, Forbes, et al., 2017). For the plasma

production process, the fundamental parameters are the solar irradiance (photon flux versus wavelength) impinging upon the atmosphere, the solar zenith angle (SZA) at a particular location, and the number density of the dominant gas to be ionized (CO_2). For a given day, solar irradiance is typically considered constant (except, of course, for solar flare studies), and thus temporal changes in solar-driven production from the dawn-to-dusk hours are due mainly to changes in SZA. The neutral atmosphere changes over a local time day, but at the heights of peak production of the M1 and M2 layers, daytime changes in CO_2 densities are small in comparison to SZA effects. Nevertheless, it is important to remember that ionospheric variability can also result from neutral atmosphere variability due to waves, winds and tides.

For the introductory version of MIRI (Mendillo et al., 2013), with its goal of specifying only N_mM_2 values, the solar radio flux at the wavelength of 10.7 cm (designated F10.7) was used to represent the solar EUV irradiance. Prior to the arrival of the Mars Atmosphere and Volatile EvolutioN (MAVEN) spacecraft at Mars (Jakosky, 2015), the choices were either F10.7 or EUV observations made at 1 AU. The now available MAVEN EUVM (Eparvier et al., 2015) observations provide daily irradiances at Mars to use in ionospheric studies, as done for quiet-sun/ non-flare times (Mendillo, Narvaez, Vogt, Mayyasi, Forbes, et al., 2017). Nevertheless, for a consistent treatment of current and past data sets, we will continue to use F10.7 as the proxy for solar irradiance.

3.1 Analysis method

The original formulation and testing of a Mars Initial Reference Ionosphere (MIRI) model is described in Mendillo et al. (2013), with only a brief summary given here. With the goal of specifying N_mM_2 values over solar zenith angles 0^o-90^o, the database used for MIRI-2013 came from the Mars Advanced Radar for Subsurface and Ionosphere Sounding (MARSIS) instrument on the Mars Express (MEX) mission (Picardi et al., 2005). The MARSIS mode called Active Ionospheric Sounding (AIS) consists of the classic ionosonde method of determining peak plasma density of the M2-layer from its critical (penetration) frequency (Gurnett et al., 2005). The total number of MARSIS/AIS observations of N_mM_2 was 112,718 values between 2005-2012, spanning solar flux F10.7 values of ~70 – 150 at 1 AU.

To relate solar fluxes measured at Earth to ionospheric observations made at Mars, the positions of both planets in their elliptical orbits must be taken into account. The protocol adopted was to transform all observations to an equivalent circular orbit for Mars (1.524 AU), and use the PCE equations at that fixed distance from the Sun to formulate the model. For each day of an observation at Mars, the following steps are done:

a. Determine the date when the side of the Sun facing Mars was observed at Earth in order to select the appropriate daily value of F10.7 to use. This is called "the rotated Sun date" – a correction that can span ± 14 days (being zero when Mars is in opposition).

b. Convert the observed flux at Earth to its equivalent value at d =1.524 AU using the $1/d^2$ correction for sunlight.

c. Transform the observed F10.7 value on the rotated Sun date to an effective solar flux (F_{eff}) obtained by smoothing the daily value with a three solar rotation (81-day) average:

$$F_{eff} = \frac{F10.7_{(day)} + \langle F10.7 \rangle_{(81-day)}}{2} \quad (1)$$

d. Convert the values of N_mM_2 observed at distance (d) to their representative values at d = 1.524 AU using the PCE equation $N_e \sim 1/d$ (Mendillo et al., 2003).

$$N_mM_2(1.524AU) = N_mM_2(d) \times d(AU)/1.524 \quad (2)$$

e. Use the derived values F_{eff} and N_mM_2 at d = 1.524 AU and cos(SZA) in the PCE equation

$$N_mM_2 \sim \sqrt{F_{eff} \times \cos(SZA)} \quad (3)$$

to determine the functional form of the correlation that can be used as the basis of the MIRI model [see Rishbeth and Garriott (1969) and Mendillo, Narvaez, Vogt, Mayyasi, Forbes, et al., (2017) for derivation of equation (3)]. We do not use the grazing incidence formula in place of cos(SZA) because it requires prior knowledge of the scale height of the neutral atmosphere (Rishbeth and Garriott, 1969). For MIRI-2013, equation (3) was calibrated using the N_mM_2 value within the data bin with the greatest number of values of SZA and F_{eff}.

For the MIRI-2018 model to be described in the next section, the relationship sought will be of the form

$$N_mM_2 = C_1\sqrt{F_{eff} \times \cos(SZA)} + C_2 \quad (4)$$

with the solar drivers for PCE conditions designated as by the parameter

$$P_{sun} = \sqrt{F_{eff} \times \cos(SZA)} \quad (5)$$

The benefit of using the equation (4) approach is that all available values of N_mM_2, F_{eff} and SZA are taken into consideration in deriving the constants C_1 and C_2. This offers a more comprehensive statistical approach to correlations. Moreover, it provides a "default" value of N_mM_2 between sunset and dawn ($N_mM_2 = C_2$, when the cosine term (with SZA = 90°) eliminates the first term in the equation).

f. Thus, for any day, MIRI computes the predicted N_mM_2 value at d = 1.524 AU for the known (or estimated) solar flux and zenith angle. It then converts that answer to Mars' distance d(AU) for that day using the inverse of equation (2).

In summary, the MIRI-2013 model embodied a coding of the above scheme (equations 1-3) to yield a prediction of N_mM_2 available at a public website (http://sirius.bu.edu/miri/miri.php). Its validation was described in Table 1 and Figures 3 and 4 in Mendillo et al. (2013).

3.2 Extending MIRI from N_mM_2 to a full $N_e(h)$ profile.

Research interest in the Martian ionosphere extends to altitudes above and below the height of maximum electron density (h_{max}). To provide estimates of the full electron density profile, a MIRI predicted N_mM_2 value was used to calibrate a normalized $N_e(h)$ profile, i.e., one extending from 80 km to 400 km with its N_mM_2 peak density value of unity. Radio occultation methods provide such profiles with clearly visible M1- and M2-layers (Hinson et al., 1999; Pätzold et al., 2005). Yet, due to the very nature of Mars-Earth occultation geometry, such databases are dominated by observations made close to solar-terminator conditions (high solar zenith angles). With MIRI's goal of predictions over the full 0°-90°

SZA range, the only choices for normalized $N_e(h)$ profile shapes are (a) use a comprehensive set of simulations or (b) use observations that sample portions of electron density profiles over a broad range of SZA conditions. Our first attempt used model profiles for SZA = 0° to 90° obtained from the Boston University Mars Ionosphere Model described in Mayyasi and Mendillo (2015). The theoretical profiles were normalized to unity at h_{max} and subsequently re-calibrated by the MIRI-2013 predictions for N_mM_2 for a given day. This comprised the MIRI-2015 model.

Validation attempts using MAVEN observations of electron density and total ion composition throughout the topside ionosphere ($h > h_{max}$) revealed an over-estimation by MIRI-2015 (Mendillo et al., 2015). The BU Model offers a 1-dimensional simulation that includes only vertical plasma diffusion above h_{max}. In reality, there is horizontal transport from the dayside to nightside. Daytime plasma profiles from MAVEN exhibited a far steeper topside gradient than shown by the 1-D model, and thus we concluded that use of a 1-D theoretical model for $N_e(h)$ profile shapes for regions above h_{max} was not fruitful.

Turning to the empirical representation of the topside ionosphere in the model by Němec et al. (2016) resulted in better agreement with MAVEN results (Mendillo, Narvaez, Vogt, Mayyasi, Mahaffy, et al., 2017). To achieve full altitude coverage in MIRI, we took the normalized shapes of the Němec et al. (2016) profiles above h_{max} for all SZAs and merged them with the normalized shapes of the theoretical profile below h_{max} for all SZAs. These are shown as Figure 1. We then calibrated the resultant $N_e(h)$ profile by the MIRI-2013 prediction of N_mM_2. The final $N_e(h)$ profile was also integrated with height to form total electron content (TEC) values. This was the status of the MIRI-2017 initiative at the onset of 2018.

4 Upgrade to Calibration Method at h_{max}

The MARSIS/AIS instrument continued to gather observations beyond the period used to formulate the initial three versions of MIRI (the 112,718 data points for SZA < 90° for 2005-2012). Here we use 223,039 observations with SZA < 90° over the years 2005-2015. Histograms of distributions of N_mM_2 values, solar fluxes, SZAs, latitude and longitude appear in Figure S1 in Supporting Information. Following the protocol given in Section 3.1 above, the results of our analysis using equation (4) appear in Figure 2. As can be seen, the application of equation (4) to the full data set gave an excellent linear correlation between N_mM_2 and the solar driven PCE parameter P_{sun}. Yet, the correlation line departs significantly from the data points in the extreme lower left portion of the figure. We considered a separate linear correlation for this region that could be merged with the linear fit at the $P_{sun} = 2$ point in the graph. For reasons to be described more fully below, we discarded that approach since it implied two PCE domains: one when P_{sun} was small due to high SZA and low F_{eff}, and one for all other conditions. Moreover, instrument issues due to course frequency resolution and signal attenuation below 2.5 MHz contribute to the odd pattern below $P_{sun} = 2$ (see Supporting Information).

To begin that discussion, we first describe the notation used along the horizontal axis in Figure 2. The P_{sun} parameters defined in equation (5) appear using integer units that result from the square root of the product of two terms. The first term is the proxy for solar irradiance that is derived from the observed solar radio flux (F10.7) at Earth—observations characterized by a two- or three-digit number (in units of 10^{-22} W/m^{2}Hz that have no relevance to atmospheric physics). The cosine term is necessarily less than 1.0, and thus the square root of the solar drivers appears as values between 0 and 8 units that have no physical meaning. They are, nevertheless, useful for discussions of ranges of observations. For

example, the tick marks on the horizontal axis at every 0.5 units of the P_{sun} parameter define regions with different statistical significance. In Table 1 we show for each bin its average value and standard deviation (1-sigma, σ). Prior to calculating the linear correlation, data points beyond 2σ for each bin (assuming a normal distribution of such a large database) were deleted (eliminating 3.2% of the points as outliers). Figure 2 thus shows results using 215,818 data points out of a total of 223,039 observations. The equation of the linear fit and its correlation coefficient (CC) is

$$N_m M_2(10^4\ e^-/cm^3) = 2.23[F_{eff} \times \cos(SZA)]^{1/2} + 1.28 \quad [CC=0.93] \qquad (6)$$

With our main focus for MIRI-2018 being the climatological behavior of N_mM_2 versus solar drivers, the statistical outliers deleted (defined as > 2σ) pertain to a small portion of the data and thus can be safely ignored (see Supporting Information). The set of scattered points in bins 6 to 8 in Figure 2 are within their 2σ bin values, and thus retained. Both types of outliers represent information relevant to instrument performance, as well as to physically-meaningful sources of ionospheric variability on day-to-day time frames. They will be treated in subsequent studies.

To emphasize that the derived relation is robust, if all data are used (i.e., with no editing to exclude outliers), the total of 223,039 N_mM_2 observations result in the following correlation:

$$N_m M_2(10^4\ e^-/cm^3) = 2.10[F_{eff} \times \cos(SZA)]^{1/2} + 1.6 \quad [CC=0.84] \qquad (7)$$

shown graphically in Figure S2 of Supporting Information. The MARSIS/AIS data set is thus dominated overwhelmingly by reliable, statistically coherent data values.

For MIRI-2018, we adopt equation (6) for the new calibration values at h_{max} for the prediction of electron density profiles. To have an uncertainty for each model prediction, we use the standard deviations of each bin of the photo-chemical parameter (P_{sun}) depicted in Figure 2 and summarized in Table 1. For the last two bins, data points are almost all from outliers and thus mean values and standard deviations are not plotted in Figure 2.

5 MIRI Module for Total Electron Content (TEC)

Total Electron Content (TEC) is defined as the integral of an electron density profile

$$TEC = \int N_e(h)\, dh \qquad (8)$$

TEC units are column contents and the convention for TEC units adopted for Mars has 1 TECU $=10^{15}\ e^-/m^2$. Sub-solar maximum values are typically ~10 TECU, with nighttime values < 1 TECU. TEC observations provide an excellent way to characterize the full vertical ionosphere on Mars. Our initial attempt to form TEC values was simply to integrate the $N_e(h)$ results from the MIRI-2017 predictions described above. The validation of this approach pointed out that MIRI's TEC values were higher than those from MAVEN for the topside contribution to TEC, i.e., when the integral in equation (8) was from h_{max} to 400 km (see Table 1 in Mendillo, Narvaez, Vogt, Mayyasi, Mahaffy, et al., 2017). The difference for midday conditions was typically a few TECU, and therefore > 20%. This is larger than uncertainties in peak density, and thus an alternate approach for TEC was adopted using a new data base.

TEC data set from the SHAllow RADar (SHARAD) on the Mars Reconnaissance Orbiter (MRO) (Campbell et al., 2013) provided 172,808 TEC values (SZA=0 ^{o} - 100 ^{o}),

spanning the period December 2006 to October 2014. 127,109 of those had a SZA < 90°. The MRO spacecraft is in a circular orbit at an altitude of 270 km around Mars, and thus the TEC integral is fixed, i.e., from ~80 km to 270 km. This height span is dominated by plasma under PCE conditions (h < 200 km), and thus the same methods described for the analysis of N_mM_2, equations (1), (2) and (4) above, can be used to derive an expression for TEC versus solar drivers. The results are shown in Figure 3 (taken from Mendillo, Narvaez, & Campbell, 2017). The correlation relationship is:

$$\text{TEC}\ (10^{15}\ \text{e}^-/\text{m}^2) = 1.23[\text{F}_{\text{eff}} \times \cos(\text{SZA})]^{1/2} + 0.73 \qquad [\text{CC}=0.96] \qquad (9)$$

MIRI-2018 now includes this SHARAD TEC Module on its website as an independent estimate of TEC.

6 Comparisons and Validations

The MIRI-2018 predictions of N_mM_2, the full $N_e(h)$ profiles, and the TEC values of the Martian ionosphere come, respectively, from observations made by MARSIS/AIS on Mars Express, the shapes of $N_e(h)$ profiles from merged empirical and theoretical models, and the TEC values from the SHARAD instrument on Mars Reconnaissance Orbiter. The task of finding new independent data sets for comparisons of predictions and observations is most easily done using radio occultation experiment (ROX) data sets. These provide $N_e(h)$ profiles from which N_mM_2 values can be extracted and TEC values can be formed via integration. ROX data sets from the Mars Global Surveyor (MGS) mission were, in fact, the primary validation source used for the original MIRI (Mendillo et al., 2013). The limitation of MGS ROX profiles is that they are typically obtained for conditions near dawn and dusk, and therefore provide tests primarily for high solar zenith angles.

The most comprehensive set of ionospheric diagnostic instruments at Mars are found on the MAVEN satellite. In-situ observations of ionospheric properties occur on every orbit segment below 400 km. Yet, with periapse usually at ~150 km, augmented by occasional "Deep-Dip" excursions to ~130 km, the full electron density profile and N_mM_2 values are not measured by the Langmuir Probe (Andersson et al., 2015) nor the ion mass spectrometer (Mahaffy et al., 2014). However, since July 2016 a radio occultation science experiment (ROSE) was implemented with MAVEN (Withers et al., 2017). In its first year of operation, a total of 48 $N_e(h)$ profiles were obtained from 5 July 2016 to 27 June 2017 (see Table S1 in Supporting Information). These are the most recent $N_e(h)$ profile observations available for MIRI validation studies, and we will use them as our primary validation source for MIRI-2018.

Another independent and earlier set of Mars Radio Science (MaRS) profiles are available from the Mars Express (MEX) mission (Pätzold et al., 2005). A sub-set of those $N_e(h)$ profiles were used to describe peak density and TEC for SZA conditions between ~100°-120° (Withers et al., 2012). These observations pertain to the nightside ionosphere and can be used to assess the C2 terms in equation (6) for N_mM_2 and equation (9) for TEC when SZA ≥ 90° cannot be used in the cos(SZA) function. We will use these Withers et al. (2012) results from MEX as a secondary source of validation.

6.1 Maximum Electron Density: Predictions and Observations

The new ROSE $N_e(h)$ profiles from MAVEN span the period 5 July 2016 to 27 June 2017. Of the 48 profiles obtained, 37 were "daytime" (SZA < 90°), 10 have SZA ≥ 90° and one had data only above 400km (excluded from analysis). A major benefit of this set of radio occultation experiments is the fact that the range of SZA was unusually broad (SZA =

49.2° to 100.4°). The comparison of the N_mM_2 values from MAVEN/ROSE and those from the new MIRI-2018 predictions appear in Figure 4a. The horizontal axis is profile number (taken from table S1 showing dates, as given in Supporting Information). The MAVEN values are shown using red dots. The MIRI predictions appear as green dots. A blue circle identifies those values with SZA ≥ 90°. MIRI's constant N_{max} value for SZA ≥ 90° is given by the dashed blue line at the bottom of the panel. The uncertainty in electron density values in ROX profiles is typically 3000 e^-/cm^3 (Hinson et al., 1999), while the uncertainty in MIRI predictions (defined as the 1σ values in Table 1) scale with N_mM_2 magnitude. As can be seen, there is good agreement between the new MAVEN/ROSE values of peak electron density and the predictions from MIRI-2018. The progression from left to right (high to low daytime magnitudes) results from both solar fluxes that decrease with time, while the SZA values increase. That is, the ROSE data set begins with close to mid-day observations and ends with near terminator conditions.

While MIRI-2018 is intended for daytime conditions, the linear fit for PCE conditions shown in equation (4) has a constant default value when the SZA ≥ 90°. The MIRI prediction (equation 6) is the constant value of $N_mM_2 \sim 1 \times 10^4$ e^-/cm^3 shown as the dashed blue line in Figure 4a. The ten MAVEN/ROSE profiles with SZA > 90° have the following average values: $\langle SZA \rangle = 95°$ and $\langle N_mM_2 \rangle = 2.25 \pm 0.99 \times 10^4$ e^-/cm^3. From the analysis of MEX/ROX nighttime N_mM_2 values in Withers et al. (2012), their Figure 4 gives peak density values of ~1.5×10^4 e^-/cm^3 for SZA = 100°. Thus the MIRI-2018 default value for beyond terminator conditions (SZA ≥ 90°), namely, the C2 terms in equation (6) or equation (7), are in reasonable agreement with relevant observations.

6.2 Total Electron Content: Predictions and Observations

We integrated the 47 profiles from MAVEN/ROSE between the altitude limits of 80 km and 270 km in order to span the same altitude range of TEC from MRO/SHARAD. The results are given in Figure 4b (shown with red dots). For comparison with MIRI, we use the two methods described above for TEC predictions: (a) integration of the MIRI $N_e(h)$ profiles (with results shown using black dots), and (b) the prediction scheme derived from SHARAD TEC observations (given by green dots). The $N_e(h)$ profile shapes (calibrated by the MIRI N_mM_2 values) clearly over-estimate TEC for all three observational periods. As mentioned above, SZA values are lower (mid-afternoon) for the first two periods, but approach 90° for the third. Prior to MAVEN, virtually all theoretical models of the Martian ionosphere used radio occultation profiles as their validation goal. This focused validation upon high SZA values. Ways to handle both primary and secondary ionization for the M1-layer was of major concern due to uncertainties in soft X-ray irradiances, cross-sections and secondary ionization rates. Success for the M1-layer was achieved in many models for these high SZA conditions (Fox et al., 1995; Martinis et al., 2003; Fox, 2004; Fox &Yeager, 2006; Mendillo et al., 2011). Applying the same secondary ionization parameterization found for high SZA conditions to cases of low SZAs was never fully explored because of the complete lack of N_mM_1 data for SZA < ~45° (Mayyasi & Mendillo, 2015).

Inspection of the bottomside profiles shown in Figure 1 suggests that the contributions of the M1-layer to TEC are overestimated for low SZA conditions. This results in MIRI's profile-integrated TEC values (black dots) being ~2 TECU above the ROSE data points. From the normalized profiles shown in Figure 1 for SZA = 0° – 40°, the TEC from heights between 80 and 105 km contributes 24% to the full TEC versus 12% for SZAs in the 70°-80° range. For ROSE profiles with $\langle SZA \rangle$ = ~50°, observed TEC = 8 TECU while MIRI profiles yield 10 TECU. Yet, the SHARAD-based MIRI TEC equation values (green dots) show far better agreement. We conclude that the secondary ionization process for small SZA

conditions is the major uncertainty for $N_e(h)$ values remaining to be solved, with topside shape parameterization now a secondary issue.

For the nighttime conditions of SZA ≥ 90°, the constant term in equation (9) is C2 = 0.73 TECU. The 10 values of TEC from MAVEN/ROSE have a sample average of 1.35 ± 0.95 TECU. In the Withers et al. (2012) analysis of MEX/MaRS nighttime results, their Figure 5 gives TEC ~ 1 TECU for SZA = 100°. Thus, C2 ~ 1 TECU term in equation (9) is a reasonable representation for beyond terminator TEC values from MIRI-2018.

6.3 MIRI Predictions from Multi-parameter Input

The fundamental approach adopted for MIRI was to predict ionospheric quantities at Mars using the equations of photo-chemical-equilibrium (PCE) to relate electron density and TEC observations at Mars to solar flux conditions measured at Earth. The MAVEN mission is the first to make solar irradiance measurements at Mars, together with electron density, electron temperature, ion densities and neutral composition. These new observations during MAVEN's "Deep Dip" campaigns to heights near h_{max} (~130 km) allow more of the PCE parameters to be included in a semi-empirical formulation. For example, 56 profiles of N_e, T_e, and $n(CO_2)$, together with solar observations, from the daytime Deep Dip period in April 2015 were used to probe the causes of ionospheric variability at Mars (Mendillo, Narvaez, Vogt, Mayyasi, Forbes, et al., 2017). As shown in that paper, an expanded version of equation (3) can be used:

$$N_e^2 \approx F_{sun}\ \cos(SZA)\ n(CO_2)(T_e)^{0.7} \qquad (10)$$

where N_e is electron density in units of e^-/cm^3, $n(CO_2)$ is number density of CO_2 in units of $\#/cm^3$, and T_e is electron temperature (°K). In place of the F10.7 parameter F_{eff} for the "rotated Sun" date (equation 1), observations from the MAVEN EUVM instrument (Thiemann et al., 2017) provide the daily solar irradiance (photon energy flux vs. wavelength) at Mars. For the M2-layer, the EUV irradiance at the top of the atmosphere (~400 km), summed over the 0.5-90 nm range, was used (in units of $10^{-3}W/m^2$). The results in Mendillo, Narvaez, Vogt, Mayyasi, Forbes, et al., (2017) for N_e at = 135 km can be taken as a first approximation for N_mM_2 when these four measured-at-Mars parameters are available:

$$N_e(10^5\ e^-/cm^3) = [1.19 + 1.74(\text{Irradiance} \times \cos(SZA) \times n(CO_2) \times (T_e)^{0.7})]^{1/2} \qquad (11)$$

with a correlation coefficient of 0.85. We now include this relationship on the MIRI-2018 site as an option when the full set of PCE parameters (irradiance, SZA, n(CO2) and T_e) are available to estimate the value of N_mM_2.

7 Summary

The concept of a "reference ionosphere" for Earth dates to the earliest days of the space age when two scientific organizations (COSPAR and URSI) embarked on a joint effort to produce an International Reference Ionosphere (IRI, https://iri.gsfc.nasa.gov). For Mars, MIRI addresses the goals and uses satisfied by the Earth's IRI—ranging from improved understanding of physical mechanisms, to providing the initial conditions for theoretical global models, and the validation of new observations. In addition, MIRI can provide engineering/applications information for programs/technologies influenced by ionospheric

parameters (e.g., radio propagation effects) and the design goals for new diagnostic instruments.

With COSPAR's expressed interest in considering certification of a Mars International Reference Ionosphere (https://cosparhq.cnes.fr/scientific-structure/scientific-commissions-c) the current efforts adopted the acronym MIRI with the "I" (for "Initial") as a place-holder for ultimate success. MIRI has already been used for some of the goals stated above. For example, when studies of MAVEN's initial data sets suggested a need for refined calibrations (Mendillo et al., 2015), revisions led to an improved understanding of day-to-day variability (Mendillo, Narvaez, Vogt, Mayyasi, Forbes, et al., 2017). Plans for a global navigation satellite system (GNSS) at Mars also require an ionospheric specification model (Mendillo et al., 2004). For the MIRI-2018 version described in this paper, improved specifications of peak density (N_mM_2) and total electron content (TEC) have been achieved. The remaining task is to provide electron density profiles $N_e(h)$ with quantitative values that yield the TEC results already available from SHARAD. As described above, the contributions to TEC from the electron densities at heights below the altitude of maximum density ($h < h_mM_2$) define the additional research goal required.

The data bases used to date are summarized in Table S2 in Supporting Information. No satellite at Mars makes *in-situ* observations of the M1-layer (80-120 km), and thus radio occultation experiments (ROX) remain the only source of such data. The new ROSE capability on MAVEN offers sampling options away from the terminator conditions that dominate ROX data sets from MGS and MEX. Coupled with new observations, additional theoretical and simulations efforts are needed to extend secondary ionization models to small SZA conditions, and to develop parameterization routines for the results obtained.

Acknowledgments

This work was supported, in part, by the MAVEN/ROSE contract to Boston University (#1546525, PW/PI) and by the NASA MDAP grant (NNX15AM46G) for analysis of MRO/SHARAD data (MM/PI). We also acknowledge the Smithsonian Institution for their contribution of the MRO/SHARAD data, which are publicly available through the geosciences node of NASA's Planetary Data System at http://pds-geosciences.wustl.edu/. The MARSIS/AIS data used for this study can also be found through the same node and website. The MAVEN data are available to the public through the NASA Planetary Data System at https://pds.nasa.gov/. F. Němec acknowledges the support of the MSMT INTER-ACTION grant LTAUA17070.

References

Andersson, L., Ergun, R. E., Delory, G. T., Eriksson, A., Westfall, J., Reed, H., … Meyers, D. (2015). The Langmuir probe and waves (LPW) instrument for MAVEN. *Space Science Reviews*, 195, 173-198. https://doi.org/10.1007/s11214-015-0194-3

Bauer, S. (1973), *Physics of Planetary Ionospheres*, Springer-Verlag, Berlin.

Bougher, S., Pawlowski, D., Bell, J. M., Nelli, S., McDunn, T., Murphy, J. R., … Ridley, A. (2015). Mars global ionosphere-thermosphere model: Solar cycle, seasonal and diurnal variations of the Mars upper atmosphere. *Journal of Geophysical Research: Planets*, 120, 311-342. https://doi.org/10.1002/2014JE004715

Campbell, B., Putzig, N., Carter, L., Morgan, G., Phillips, R., & Plaut, J. (2013). Roughness and near-surface density of Mars from SHARAD radar echoes. *Journal of Geophysical Research*, 118(3), 436–450. https://doi.org/10.1002/jgre.20050

Chaufray, J.-Y., Gonzalez-Galindo, F., Forget, F., Lopez-Valverde, M., Leblanc, F., Modolo, R., … Witasse, O. (2014). Three-dimensional Martian ionosphere model: II. Effect of transport processes due to pressure gradients. *Journal of Geophysical Research: Planets*, 119, 1615-1636. https://doi.org/10.1002/2013JE004551

Eparvier, F. G., Chamberlin, P. C., Woods, T. N., & Thiemann, E. M. B. (2015). The Solar Extreme Ultraviolet Monitor for MAVEN. *Space Science Reviews*, 195, 293–301. https://doi.org/10.1007/s11214-015-0195-2

Fox, J. (2004). Response of the Martian thermosphere/ionosphere to enhanced fluxes of solar soft X-rays. *Journal of Geophysical Research: Space Physics*, 109, A11310. https://doi.org/10.1029/2004JA010380

Fox, J. L., & Yeager, K. E. (2006). Morphology of the near-terminator Martian ionosphere: A comparison of models and data. *Journal of Geophysical Research*, 111, A10309. https://doi.org/10.1029/2006JA011697

Fox, J., Zhou, P., & Bougher, S. (1995). The Martian thermosphere/ionosphere at high and low solar activities. *Advances in Space Research*, 17(11), 203-218. https://doi.org/10.1016/0273-1177(95)00751-Y

Gurnett, D., Kirchner, D. L., Huff, R. L., Morgan, D. D., Persoon, A. M., Averkamp, T. F., … Picardi, G. (2005). Radar soundings of the ionosphere of Mars. *Science*, 310(5756), 1929–1933. https://doi.org/10.1126/science.1121868

Hinson, D., Simpson, R., Twicken, J., Tyler, G., & Flasar, F. (1999). Initial results from radio occultation measurements with Mars Global Surveyor. *Journal of Geophysical Research*, *104*(*E11*), 26,997–27,012. https://doi.org/10.1029/1999JE001069

Jakosky, B. (2015). MAVEN explores the Martian upper atmosphere, *Science*, 350(6261), 643. https://doi.org/10.1126/science.aad3443

Ma, Y., Nagy, A., Sokolov, I., & Hansen, K. (2004). Three-dimensional, multispecies, high spatial resolution MHD studies of the solar wind interaction with Mars. *Journal of Geophysical Research: Space Physics*, 109, A07211. doi:10.1019/2003JA010367

Mahaffy, P. R., Benna, M., King, T., Harpold, D. N., Arvey, R., Barciniak, M., … Bendt, M. (2014). The neutral gas and ion mass spectrometer on the Mars atmosphere and volatile evolution mission. *Space Science Reviews*, 195, 49–73. https://doi.org/10.1007/s11214-014-0091-1

Martinis, C. R., Wilson, J. K., & Mendillo, M. J. (2003). Modeling day-to-day ionospheric variability on Mars. *Journal of Geophysical Research*, 108(A10), 1383. https://doi.org/10.1029/2003JA009973

Matta, M., Mendillo, M., Withers, P., & Morgan, D. (2015). Interpreting Mars ionospheric anomalies over crustal magnetic field regions using a 2-D ionospheric model. *Journal of*

Geophysical Research: Space Physics, 120(1), 766–777. https://doi.org/10.1002/2014JA020721

Mayyasi, M., & Mendillo, M. (2015). Why the Viking descent probes found only one ionospheric layer at Mars. *Geophysical Research Letters*, 42, 7359–7365. https://doi.org/10.1002/2015GL065575

Mendillo, M., Lollo, A., Withers, P., Matta, M., Pätzold, M., & Tellmann, S. (2011). Modeling Mars' ionosphere with constraints from same-day observations by Mars Global Surveyor and Mars Express. *Journal of Geophysical Research*, 116, A11303. https://doi.org/10.1029/2011JA016865

Mendillo, M., Marusiak, A., Withers, P., Morgan, D., & Gurnett, D. (2013). A new semi-empirical model of the peak electron density of the Martian ionosphere. *Geophysical Research Letters*, 40, 5361–5365. https://doi.org/10.1002/2013GL057631

Mendillo, M., Narvaez, C., & Campbell, B. (2017). The total electron content of the Martian ionosphere from MRO/SHARAD observations. *Journal of Geophysical Research: Planets*, 122, 2182–2192. https://doi.org/10.1002/2017JE005391

Mendillo, M., Narvaez, C., Matta, M., Vogt, M., Mahaffy, P., Benna, M., & Jakosky, B. (2015). MAVEN and the Mars Initial Reference Ionosphere model. *Geophysical Research Letters*, 42, 9080–9086. https://doi.org/10.1002/2015GL065732

Mendillo, M., Narvaez, C., Vogt, M. F., Mayyasi, M., Forbes, J., Galand, M., … Mahaffy, P. (2017). Sources of ionospheric variability at Mars. *Journal of Geophysical Research: Space Physics*, 122. https://doi.org/10.1002/2017JA024366

Mendillo, M., Narvaez, C., Vogt, M. F., Mayyasi, M., Mahaffy, P., Benna, M., … Jakosky, B. (2017). MAVEN and the total electron content of the Martian ionosphere. *Journal of Geophysical Research: Space Physics*, 122, 3526–3537. https://doi.org/10.1002/2016JA023474

Mendillo, M., Pi, X., Smith, S., Martinis, C., Wilson, J., & Hinson, D. (2004). Ionospheric effects upon a satellite navigation system at Mars. *Radio Science*, 39, RS2028. https://doi.org/10.1029/2003RS002933

Mendillo, M., Smith, S., Wroten, J., Rishbeth, H., & Hinson, D. (2003). Simultaneous Ionospheric Variability on Earth and Mars. *Journal of Geophysical Research*, 108(A12), 1432. https://doi.org/10.1029/2003JA009961

Němec, F., Morgan, D., Gurnett, D., & Andrews, D. (2016). Empirical model of the Martian dayside ionosphere: Effects of crustal magnetic fields and solar ionizing flux at higher altitudes. *Journal of Geophysical Research: Space Physics*, 121, 1760–1771. https://doi.org/10.1002/2015JA022060

Pätzold, M., Tellmann, S., Häusler, B., Hinson, D., Schaa, R., & Tyler, G. (2005). A sporadic third layer in the ionosphere of Mars. *Science*, 310(5749), 837–839. https://doi.org/10.1126/science.1117755

Picardi, G., Plaut, J. J., Biccari, D., Bombaci, O., Calabrese, D., Cartacci, M., … Watters, T. R. (2005). Radar soundings of the subsurface of Mars. *Science*, 310(5756), 1925–1928. https://doi.org/10.1126/science.1122165

Sanchez-Cano, B., Morgan, D. D., Witasse, O., Radicella, S. M., Herraiz, M., Orosei, R., … Quinsac, G. (2015). Total electron content in the Martian atmosphere: A critical reassessment of the Mars express MARSIS data sets. *Journal of Geophysical Research: Space Physics*, 120(3), 2166–2182. https://doi.org/10.1002/2014JA020630

Rishbeth, H., & Garriot, O. (1969). *Introduction to Ionospheric Physics*. *NY*: Academic Press.

Rishbeth, H., & Mendillo, M. (2004). Ionospheric layers of Mars and Earth. *Planetary and Space Science*, 52, 849–852. https://doi.org/10.1016/j.pss.2004.02.007

Thiemann, E., Chamberlin, P. C., Eparvier, F. G., Templeman, B., Woods, T. N., Bougher, S. W., & Jakosky, B. M. (2017). The MAVEN EUVM model of solar irradiance variability at Mars: Algorithms and results. *Journal of Geophysical Research: Space Physics*, 122, 2748–2767. https://doi.org/10.1002/2016JA023512

Vogt, M. F., Withers, P., Mahaffy, P. R., Benna, M., Elrod, M. K., Halekas, J. S., … Mazelle, C. (2015). Ionopause-like density gradients in the Martian ionosphere: A first look with MAVEN. *Geophysical Research Letters*, 42(21), 8885–8893. https://doi.org/10.1002/2015GL065269

Withers, P., Fillingim, M. O., Lillis, R. J., Häusler, B., Hinson, B. P., Tyler, G. L., … Witasse, O. (2012). Observations of the nightside ionosphere of Mars by the Mars Express Radio Science Experiment (MaRS). *Journal of Geophysical Research: Space Physics*, 117, A12307. https://doi.org/10.1029/2012JA018185

Withers, P., Mendillo, M., Moore, L., Felici, M., & Jakosky, B. M. (2017). Latest results from the MAVEN Radio Science Occultation Experiment (ROSE). Abstract P51C-2617 presented at 2017 Fall Meeting, AGU, New Orleans, LA, 11-15 Dec.

Table 1. Photo-chemical parameter bin average and standard deviation

PCE Bin [$10^4 e^-/cm^3$]	**mean value [$10^4 e^-/cm^3$]**	**σ [$10^4 e^-/cm^3$]**	**σ [% of mean]**
0 ≤ bin 1 < 0.5	4.2	0.76	18.07
0.5 ≤ bin 2 < 1	4.4	0.76	17.20
1 ≤ bin 3 < 1.5	4.9	0.77	15.84
1.5 ≤ bin 4 < 2	5.4	0.68	12.62
2 ≤ bin 5 < 2.5	6.0	0.78	12.99
2.5 ≤ bin 6 < 3	6.7	0.99	14.71
3 ≤ bin 7 < 3.5	7.6	1.4	18.51
3.5 ≤ bin 8 < 4	8.9	1.7	19.08
4 ≤ bin 9 < 4.5	10.3	1.8	17.44
4.5 ≤ bin 10 < 5	11.8	1.7	14.40
5 ≤ bin 11 < 5.5	13.2	1.8	13.67
5.5 ≤ bin 12 < 6	14.2	2.1	14.81
6 ≤ bin 13 < 6.5	14.1	3.5	24.87
6.5 ≤ bin 14 < 7	13.7	4.6	33.66
7 ≤ bin 15 < 7.5	10.4	6.3	60.71
7.5 ≤ bin 16 < 8	10.1	7.5	74.32

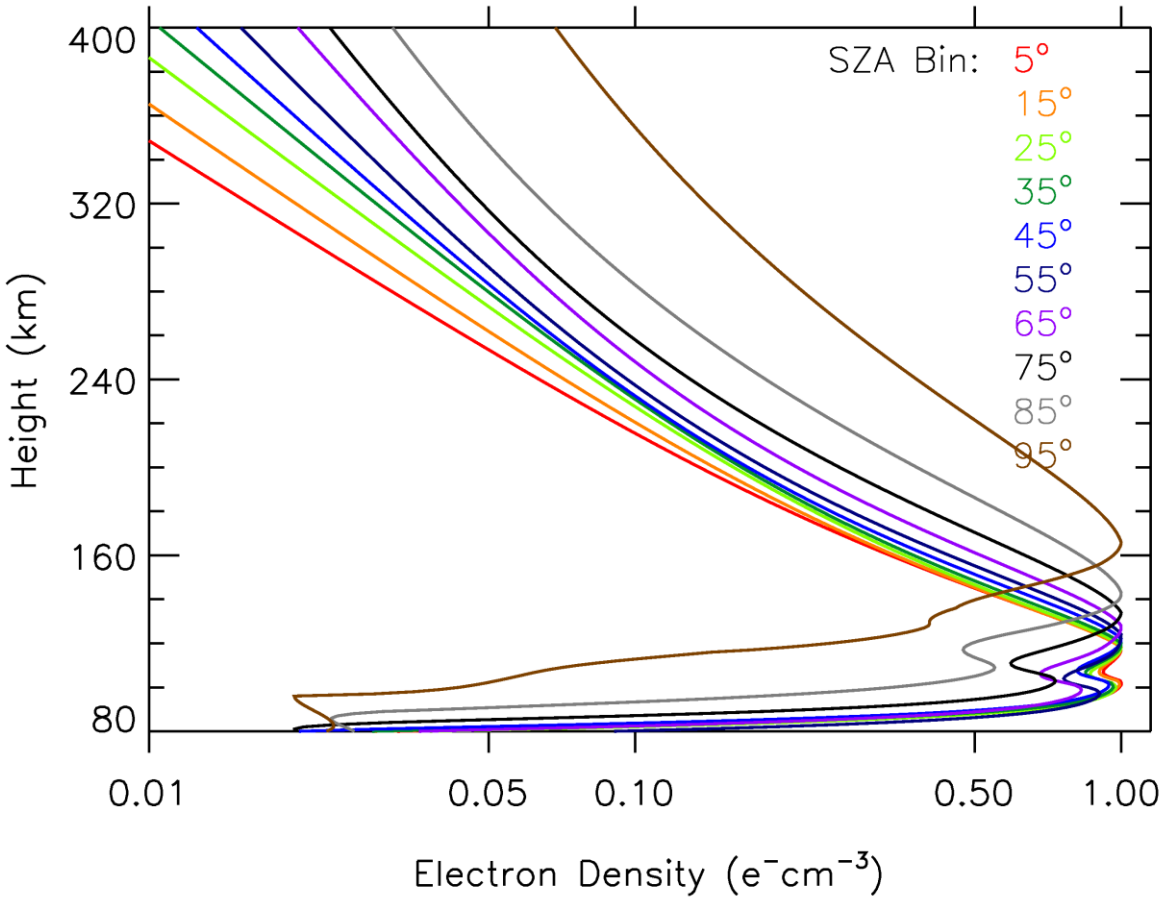

Figure 1. Electron density profiles formed by merging the topside of normalized climatological profiles (Němec et al. 2016) and the bottomside of normalized theoretical profiles (Mayyasi & Mendillo, 2015) for each solar zenith angle bin. These are calibrated by the peak density MIRI-2013 predicts.

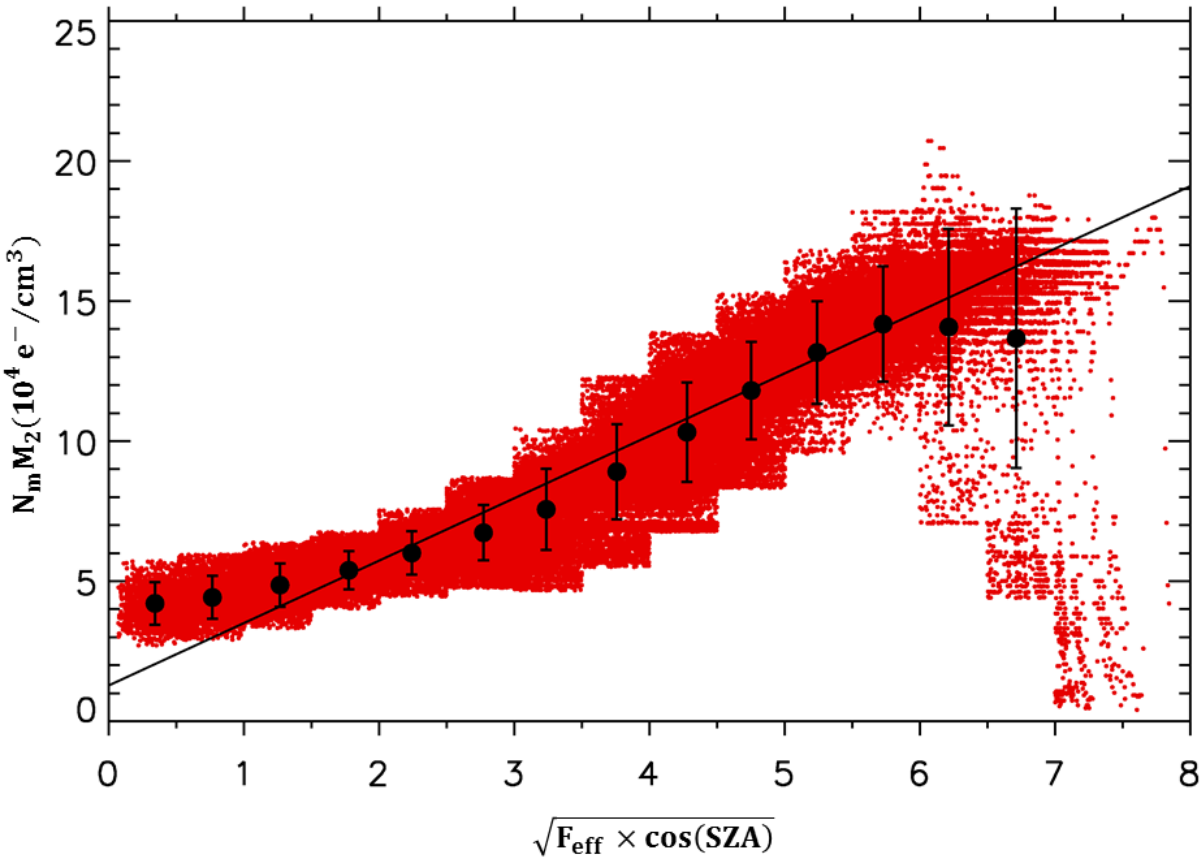

Figure 2. Correlation of N_mM_2 values (from MARSIS/AIS) with the solar parameter for photo-chemical-equilibrium [$P_{sun} = \sqrt{F_{eff} \times \cos(SZA)}$] given by equations (4) and (5), after eliminating outliers beyond 2-sigma within each P_{sun}. This data set includes 215,818 values from 2005-2015 (97% of the total available values with SZA < 90°). The best-fit equation and linear correlation coefficient (CC) are $N_m M_2 (10^4\, e^-/cm^3) = 2.23[F_{eff} \times \cos(SZA)]^{1/2} + 1.28$, with CC=0.93. See text.

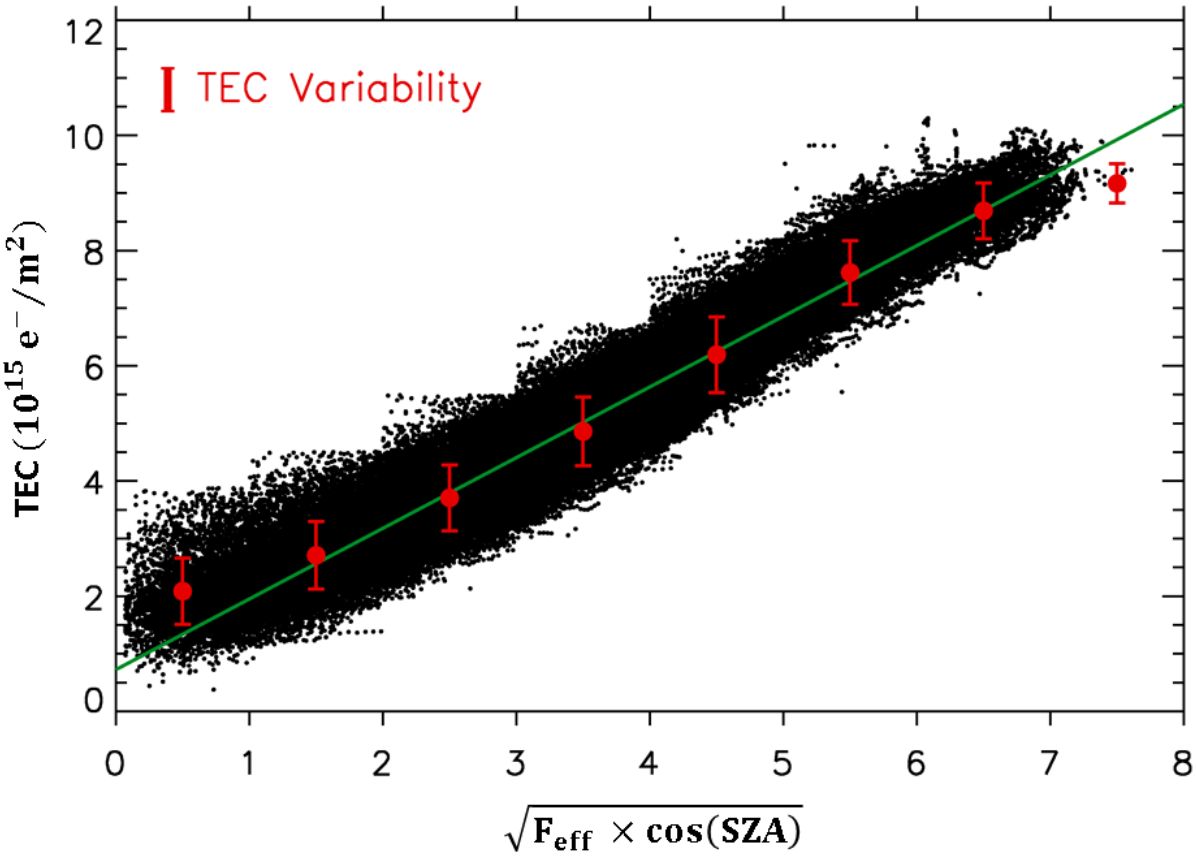

Figure 3. Correlations of Martian total electron content and solar parameters at Mars' mean orbital distance of 1.524 AU (see text). The SHARAD TEC values are shown versus the PCE parameter $\sqrt{F_{eff} \times \cos(SZA)}$ with F_{eff} as defined in equation (1). For each unit bin on the horizontal axis, mean values of TEC are shown by the red dot (with 1σ variability about that average). Of the 127,109 number of data points for SZA < 90°, 126,055 are within 2σ and are used to find the relationship and correlation between TEC and PCE parameter (taken from Figure 7 in Mendillo, Narvaez, & Campbell, 2017).

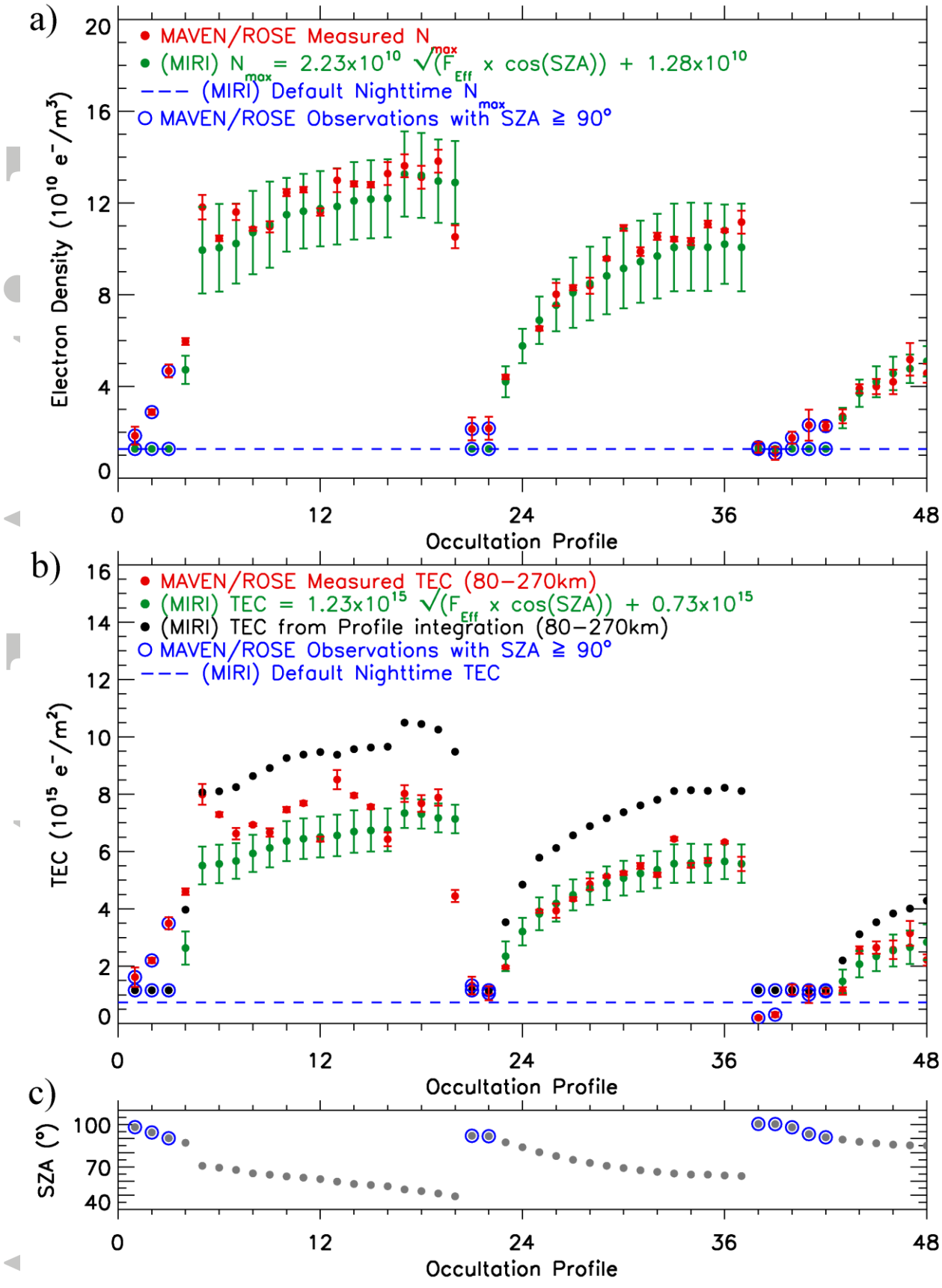

Figure 4. Comparison of MIRI-2018 predictions of electron density profile $N_e(h)$ parameters with observations made by the Radio Occultation Radio Experiment (ROSE) during the

"occultation seasons" of the MAVEN mission. (a) Maximum electron density of the M2-layer (N_mM_2). Measured values are shown with red dots. MIRI-2018 predictions for N_mM_2 use green dots. Blue circles indicate values with SZA $\geq 90^o$. MIRI's constant N_{max} value for SZA $\geq 90^o$ is shown by the blue dashed line. (b) Same color scheme of red dots for ROSE observations of TEC. There are two MIRI estimates of TEC: black dots refer to TEC from integration of MIRI N_e(h) profiles, while green dots come from the MIRI/SHARAD predictions. Blue circles indicate observations with SZA $\geq 90^o$. MIRI/SHARAD's default TEC value for SZA $\geq 90^o$ is marked by a blue dashed line. (c) Solar zenith angles for each of the profiles. SZAs $\geq 90^o$ are surrounded by blue circles. Lower SZAs correspond to higher N_mM_2 a